A NUMERICAL COMPARISON ON THE AERODYNAMIC PERFORMANCE OF A TWO-STAGE TWO-SPOOL TURBINE FACILITY PREDICTED BY STEADY AND UNSTEADY SIMULATIONS

Rosario Spataro, Emil Göttlich, Cornelia Santner, Franz Heitmeir

Institute for Thermal Turbomachinery and Machine Dynamics
Graz University of Technology, Graz, Austria, A-8010
Email: rosario.spataro@tugraz.at

ABSTRACT

The paper discusses the time-averaged and the time-resolved flow in a two-stage two-spool test rig located at the Institute for Thermal Turbomachinery and Machine Dynamics (ITTM) of Graz University of Technology. The facility consists of a transonic turbine stage followed by a counter-rotating subsonic low pressure turbine. The rig was designed and operated within the EU-project DREAM, where the target was to built up a machine able to investigate the aerodynamics of interturbine S-shaped channels. An optimized design of this component represents a critical goal for the performances of modern and future jet engines.

The turbine design techniques are nowadays still carried out by optimizations based on steady-state simulations: nevertheless since a long time it is well known how the engine performances are strongly dependent by the unsteady effects. The use of interfaces such as mixing plane or frozen rotor cuts off the real interactions between successive blade rows so that pressure losses and aeroacoustic effects are consequently estimated incorrectly. Such considerations are important for the designer who has to face a highly three dimensional unsteady flow like in a transonic turbine stage.

Therefore, the aim of the present paper is to provide a quantitative comparison in terms of performance estimation error whenever a numerical simulation is undertaken in order to catch the time-mean or the time-resolved flow.

This paper used data part of the EU-project DREAM (ValiDation of Radical Engine Architecture SysteMs, contract No. ACP7-GA-2008-211861).

NOMENCLATURE

C	low pressure vane axial chord	$n_{r,in}$	Reduced rotational speed, stage inlet
Cp_T	total pressure coefficient	p_T	total pressure
Cp	static pressure coefficient	p	static pressure
H	channel height	r	radial coordinate
HP	High Pressure	$TMTF$	Turning Mid Turbine Frame
LP	Low Pressure	v	velocity
$m_{r,in}$	Reduced mass flow, stage inlet	v_t	tangential velocity
Ma	Mach number	x	axial coordinate
α	Yaw angle (from meridional dir.)	η	efficiency

INTRODUCTION

Modern civil jet-engine companies have to face ambitious targets in terms of size and weight reduction. Therefore, over the last years, a lot of research work was put in getting beyond the standards of state-of-the-art propulsion systems.

In large engines, whenever it is required to maximize the pressure ratio at a fixed number of stages keeping adequate rotational speeds, a conventional solution is to set up the system in multi-shaft configuration (up to 3 shafts in Rolls Royce TRENT engines family). In particular, counter-rotating spools can be used to compensate the gyroscopic effect of the rotating masses as well as to minimize the aerodynamic losses in the intermediate stage (i.e. General Electric GEnx, Rolls Royce TRENT 1000, Pratt & Whitney PW1500).

In order to increase the engine bypass-ratio and, therefore, the propulsion efficiency, the fan front section has to be enlarged. This is limited by structural and acoustic limits on the fan tip velocity. At the same time, the HP-shaft rotational speed should be increased whenever a higher cycle maximum pressure is required.

The resulting larger difference in the shafts rotational speeds leads to an increasing difference in the components diameters (compressors and turbines). Therefore, focusing on the turbine, the resulting S-shaped design of the diffuser between the HP and LP turbines is quite important for the optimisation of the overall engine aerodynamic performance. Such a component is also called mid turbine frame (MTF).

Since the flow in these diffusers is highly 3D and characterized by a high content of unsteadiness, it is important for the design engineer responsible for the performance estimation to be aware of how the different CFD settings influence the solution.

Conventionally, the first step in performing blade row calculation (Tucker (2011)) is represented by the use of mixing planes interfaces.

The fidelity in modeling the steady flow within the machine could be improved using a frozen rotor interface (Tucker (2011)): here, the wakes are passed to the downstream domains, but no relative wake movement is transferred. Anyway, for a good prediction of the aerodynamic efficiency or of the acoustic tonal noise, the unsteady flow should be modeled. In fact, as noted by Meneveau and Katz (2002) and Rhie et al (1995) the unsteady stresses resulting from the movement of the wakes will be typically of a similar or higher magnitude than the turbulent stresses. Starting with Adamczyk (1985), a lot of effort was put in trying to model unsteady effects.

The use of sliding planes is necessary for prediction distortion transfer, getting the acoustics tonal noise and generally having high fidelity calculations (Tucker (2011)). Here, every timestep the rotor mesh(s) slide/rotate in the tangential direction relative to the stator(s). Modeling a real machine a problem of computational effort occurs whenever $360deg$ annulus calculation is required (including all blades). On the other hand, in order to reduce the blade count per domain passage, different hypothesis (i.e. scaling the pitch keeping the same pitch-to-chord ratio) could be stated to resize the circumferential extent.

In the last years, a lot of papers were presented on the prediction of the unsteady flow field of high pressure turbines Arnone and Pacciani (1996); Dénos et al (2001); Miller et al (2003b); Gaetani et al (2007). Lavagnoli et al (2012); Yasa et al (2011) presented an aerodynamic analysis of a low pressure vane placed in an S-shape duct downstream of a transonic turbine stage. Miller et al (2003a) used the unsteady CFD to explain the flow evolution through an inter-turbine diffuser placed downstream of a HP turbine. In none of these cases an inter-turbine diffuser was modeled between two rotors.

The machine which is object of the present paper is located at the Institute for Thermal Turbomachinery (ITTM) of Graz University of Technology. The aerodynamic design was conducted by MTU Aero Engines. Details on the test turbine can be found in Erhard and Gehrer (2000); Hubinka et al (2009, 2011). In this setup turning struts are located within the inter-turbine diffuser (turning mid turbine frame, TMTF).

Santner et al (2011) presented the influence of the HP turbine secondary flows and wakes on the TMTF. Lengani et al (2012b) showed by means of a modal decomposition analysis of the unsteady flow field that in such machines rotor-rotor interaction can be observed downstream of the LP stage.

Spataro et al (2012) discussed the flow evolution through the S-shaped channel by means of a steady simulation and showed how the structures coming from the HP stage propagates through the TMTF and their influence at the LP rotor inflow.

The aim of this work is to provide a comparison between different numerical setups, whenever the highly unsteady 3D flow field of a two-Stage two-Spool transonic turbine has to be predicted by means of simulating both stages.

EXPERIMENTAL APPARATUS AND METHODOLOGY

Facility

The transonic test turbine facility is a continuously operating two-stage cold-flow open-circuit plant, which consists of a transonic HP stage and a counter-rotating LP stage (a schematic drawing is shown in Fig. 1). Detailed information on the design and construction of the original single stage facility can be found in Erhard and Gehrer (2000). For the design of the LP-stage together with the TMTF see Hubinka et al (2009) and for the operation Hubinka et al (2011).

Table 1 summarizes the main parameters for the HP stage and the LP stage (TMTF+LP rotor) and the operating condition.

Measurement techniques

The experimental investigations were conducted by means of 5 hole probes traversed in three planes: the first one located just downstream of the HP stage (Plane C in Figure 1), the second one is located downstream of the turning LP vane (Plane E in Fig. 1), while the third plane can be found downstream of the LP rotor (Plane F in Fig. 1). Moreover one of the struts was instrumented with pressure taps along three spanwise location at 25%, 50% and 75% span. In the measurements planes the probe was traversed radially over 95% of the blade height and over one HP-vane pitch (Plane C) and over one LP-vane pitch (Planes E and F). Further details about the measurements uncertainities can be found in Santner et al (2011).

Table 1: Blading parameters and operating conditions.

Blading parameters				
	HP vane	HP blade	TMTF	LP blade
Vane/ blade no.	24	36	16	72
h/c_{ax}	1.15	1.37	0.53	2.94
Re(10^{-6})	2.38	1.1	1.86	0.46
Tip gap	-	unshrouded	-	shrouded
Operating conditions				
		HP stage	LP stage	
$n_{r,in}$ $[rpm/\sqrt{K}]$		524.4	195.3	
$m_{r,in}$ $[kg/s \cdot \sqrt{K}/(bar)]$		81.2	214.6	
Stage p_t ratio		3	1.3	
Power [kW]		1710	340	

Numerical setup

In this paper several numerical simulations with different setups are compared. The domain boundaries and the interface locations are shown in Figure 1. Four steady CFD simulations (Case A, B, C and D in Table 2) are compared with an unsteady solution (Unsteady CFD in Table 3)).

The measured field at the machine inlet was used as inlet boundary condition for the numerical simulation, while the outlet boundary was placed at an axial distance of $(x_{out} - x_{LProtor_{TE}})/C_{LProtor} =$

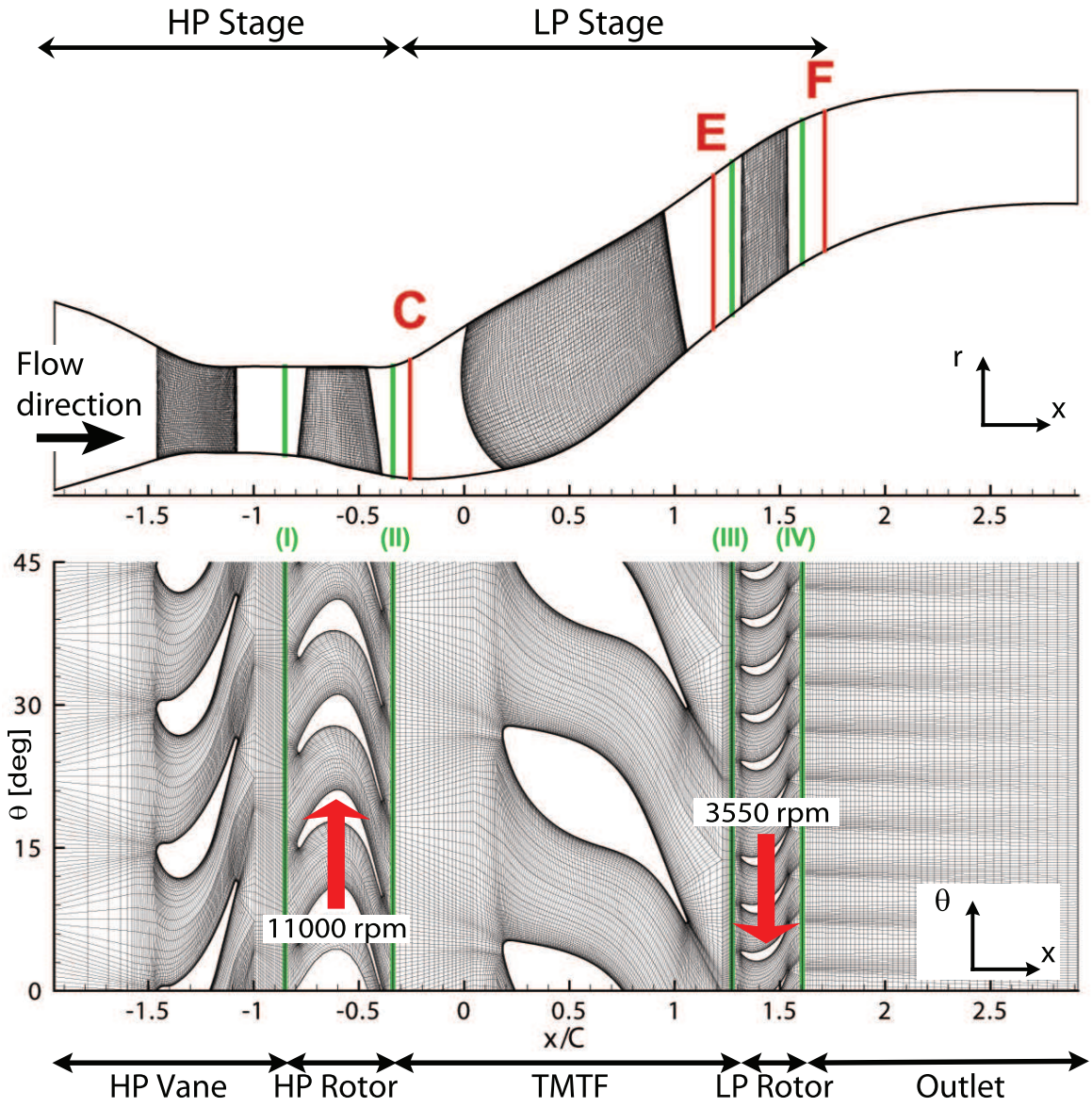

Figure 1: Two-Stage two-Spool facility at the ITTM and computational domain

6 downstream of the LP rotor trailing edge. At this coordinate static pressure taps within the facility measure the static pressure of the outflow.

The mesh was generated keeping the y^+ lower than 1 next to the blade surface and lower than 2 next to the endwalls. Details on the mesh sizes can be found in Table 2. A grid independence study was done as assumption for the numerical investigation. A commercial CFD code (Ansys CFX©v12.1) was used as solver. The code solves the Navier Stokes equation system with first order accuracy in areas where the gradients change sharply to prevent overshoots and undershoots and maintain robustness, and second order in flow regions with low variable gradients to enhance accuracy (ANSYS (2010)). The turbulence was modeled using a k-ω SST turbulence model (Menter (1994)). Before proceeding with the discussion of the results, it is important to present the differences between the setups (Table 3):

Case A In this simulation each domain consists of one blade passage mesh. The outlet domain has a pitchwise extension of 5 degrees of pitch extension (the same as the LP rotor's mesh). All interfaces (I, II, III, IV) are mixing planes.

Table 2: CFD Setups.

Mesh passage per domain and Mesh size (in million of nodes)						
	HP Vane	HP Rotor	TMTF	LP Rotor	Outlet	Tot Mesh size
Mesh size	0.67	0.39	1.03	0.23	0.06	
no. Radial points	60	60	60	60	60	
no. Blade to blade points	80	60	110	50	50	
Case A	1	1	1	1	1	2.38
Case B	1	9	4	1	1	8.59
Case C	1	1	1	1	1	2.38
Case D	1	1	1	1	1	2.38
Unsteady	6	9	4	18	18	16.87

Domain Interfaces for different numerical setups				
	(I)	(II)	(III)	(IV)
Case A	Mix pl	Mix pl	Mix pl	Mix pl
Case B	Mix pl	Frz rot	Mix pl	Frz rot
Case C	Mix pl	Mix pl	Mix pl	Frz rot
Case D	Mix pl	Mix pl	Mix pl	– (*)
Unsteady	Slide	Slide	Slide	Slide

(*) counter rotating endwalls for the downstream domain

Case B Interfaces II and IV were changed to frozen rotors. Therefore, the same periodicity is required for the HP rotor and the TMTF (90 degrees), and for the LP rotor and the outlet domain (5 degrees). Interfaces I and III were kept as mixing planes.

Case C The mesh setup for this case is the same as for Case A: interfaces I, II and III are mixing planes, while interface IV was turned to frozen rotor.

Case D For this case the mesh of the outlet domain and the one of the LP rotor were merged together removing interface IV. This leads to one rotational domain (LP rotor + Outlet) where counter rotating wall velocity was assigned to the hub and shroud endwalls in order to fix them in the absolute frame. Interfaces I, II and III are mixing planes.

Unsteady In order to simulate the time-resolved flow, an unsteady CFD was performed using sliding interfaces. Therefore it was required to satisfy the machine full periodicity computing 90 degrees for each domain. This leads to a quite heavy calculation where the mesh refinement was constrained by the server maximal memory (32 GB). The timestep was set to 1/100 of the HP rotor blade passing period ($t_s = 1.5e-6s$). The numerical scheme is time marching where the code solves second order backward equations.

RESULTS AND DISCUSSION

In this section the results from the CFD calculations are presented and compared with the experimental data. The CFD calculations were set in order to provide a guide line for engineers who face similar problems.

A first baseline configuration (Case A) is set by putting mixing planes between each domain of the setup. This is often the first choice for a steady simulation setup because of the low computational cost, and because it is thought to provide anyway a reasonable prediction even if the flow physics are not well known.

A second setup (Case B) was chosen as an alternative solution for calculating the machine performances by a steady run. Here the aim was to improve the prediction by considering the losses generated by the development of the rotors structures through the channel. Therefore two frozen rotors were placed downstream of the HP stage and of the LP rotor respectively. Such solution implies an increased computational cost due to a more extended mesh.

The third and the forth cases (Case C and D) have to be seen as two possible attempts to improve performance estimation keeping the same computational cost as Case A.

Finally, the time averaged transient data were analyzed.

A discussion is presented aimed to point out the differences between the CFD data and measurements on the machine performance evaluation. It is shown how in such a setup the prediction firstly has a significant dependency from the choice of the interface settings, and secondly evidence the importance of modeling the structures released by the rotors whenever the maximum agreement with the experiments is required.

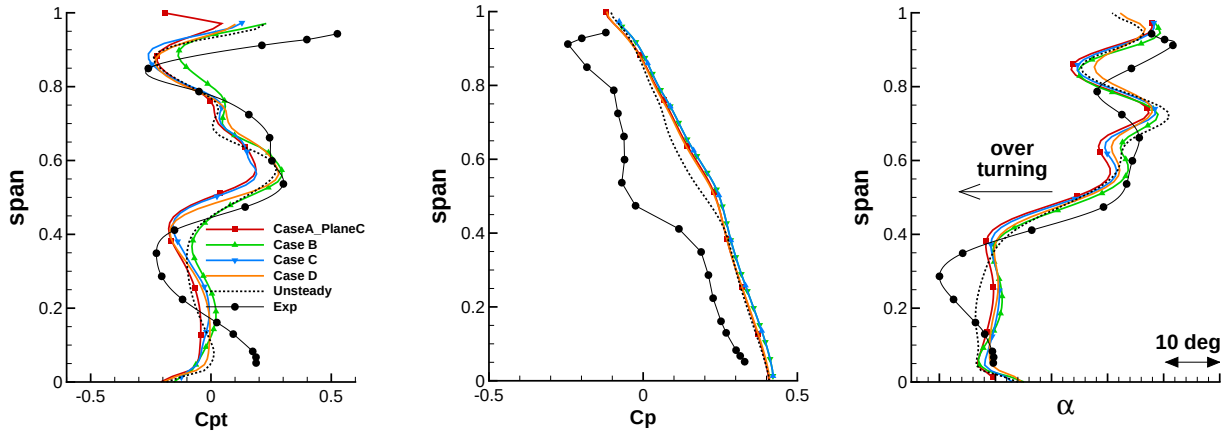

(a) Total pressure (b) Static pressure (c) Yaw angle

Figure 2: Plane C - Spanwise mass-averaged distributions at the TMTF inlet

TMTF Inflow

The upstream HP turbine is a low aspect ratio stage with an unshrouded rotor where secondary flows are predominant in the stator-rotor interaction Dénos and Paniagua (2005); Persico et al (2010).

Figure 2(a) shows a comparison of spanwise circumferentially averaged total pressure distribution between measurements (dots) and CFD cases (A, B, C, D and Unsteady).

The total pressure is plotted as total pressure coefficient Cp_T and defined as:

$$Cp_T = \frac{p_T - \bar{p}_{T,C}}{\bar{p}_{T,C} - \bar{p}_C} \tag{1}$$

where $\bar{p}_{T,C}$ and $\bar{p}_C$ are the experimental mass-weighted total pressure and static pressure in Plane C, respectively.

Figure 2(b) shows the same comparison in terms of static pressure coefficient Cp is defined as follows:

$$Cp = \frac{p - \bar{p}_C}{\bar{p}_{T,C} - \bar{p}_C} \tag{2}$$

Figure 2(c) represent the experiments-numerics comparison in terms of yaw angle (α). Experimental data show a maximum variation of the yaw angle over the channel height of about 42 deg.

The first bend of the duct induces a tip-to-hub pressure gradient (Figure 2(b)) which pushes the

low energy structures towards the shroud (wakes and passage vortices) (Figure 2(a)). For a more detailed description of the flow field of the machine in this region refer to Spataro et al (2012).

Looking at the spanwise distribution in this plane, the CFD shows a vertical shift of $r/H \approx 0.1$ in predicting the location of secondary losses. Figure 2(a) shows how problems with the simulations can be found in the lower half of the channel, where the HP stator-rotor interaction induces a loss distribution which is difficult to predict with steady solutions. Case B as well as the unsteady CFD show anyway a better agreement of the two curves in this region.

When comparing the steady solutions (Case A, B, C, D) in Figure , Case B shows an under prediction of the HP rotor tip leakage losses. Even in this case the unsteady solution shows a better agreement with the measurements. Between $r/H = 0.6$ and $r/H = 0.8$, in correspondence of the HP rotor higher passage vortex, the CFD seems over predicting the losses.

Looking at the yaw angle distribution in Figure 2(c), it is still possible to identify the vertical displacement between numerical data and measurements. Moreover, the computed HP rotor upper passage vortex is also overestimating the flow underturning between $r/H = 0.6$ and $r/H = 0.8$, while at the lower channel half the CFD underestimates the spanwise changes in flow angle. At midspan Case B (Figure 2(c)) seems to provide the best match with the experiments between the steady simulations. Looking at the shape of the curve in the lower half of the channel (where secondary vortices and stator-rotor interaction mechanism influence the distribution) the unsteady run seems to best predict the trend. This prediction problem was already observed by Wallin et al (2011) which performed numerical simulation on this machine using another setup for the TMTF.

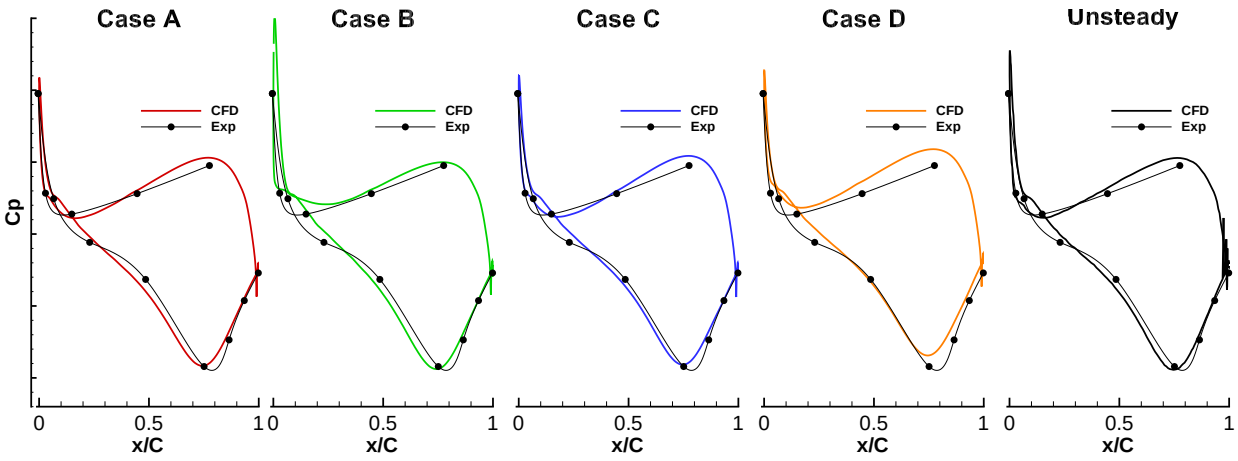

Figure 3: TMTF Blade loading at midspan

Within the TMTF passage

Moving downstream of Plane C, the flow is led towards the LP rotor by turning struts. The aerodynamics of these wide-chord vanes is quite important for the flow control within the S-shaped channel. Therefore one of these struts was instrumented with pressure taps.

Figure 3 shows the TMTF blade loading at midspan. Numerical data for each setup (A, B, C, D and Unsteady) are superimposed to the static pressure measurements. It was already observed by Santner et al (2011) that the strut at this span position faces negative flow incidence.

Case D in Figure 3 shows the worst agreement with the experimental data. The flow incidence in Case B is influenced by the frozen rotor placed between the HP rotor and the TMTF, but the dependency from the rotor-strut relative position is anyway negligible. Case B and the unsteady CFD provide the best overall prediction in terms of blade loading distribution on the vane.

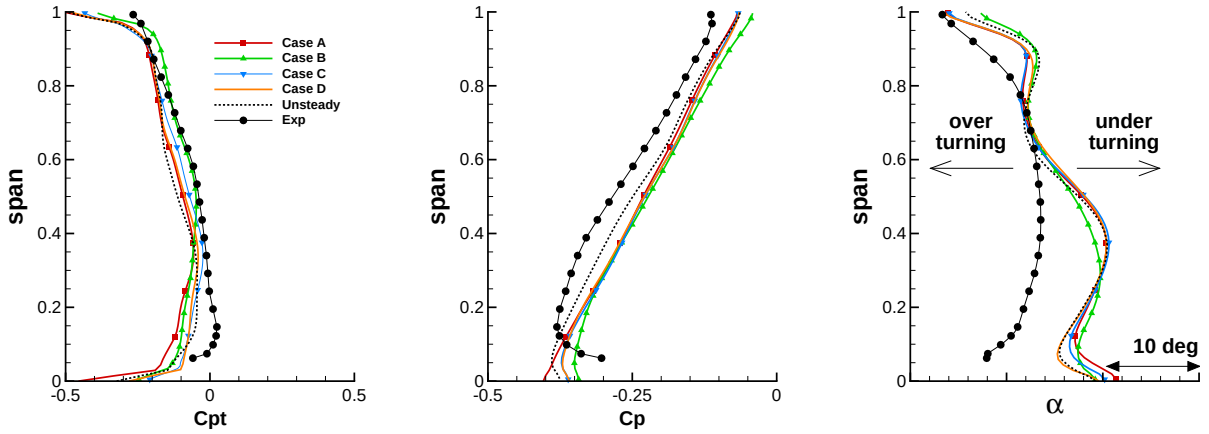

(a) Total pressure (b) Static pressure (c) Yaw angle

Figure 4: Plane E - Spanwise mass-averaged distributions at the TMTF outflow

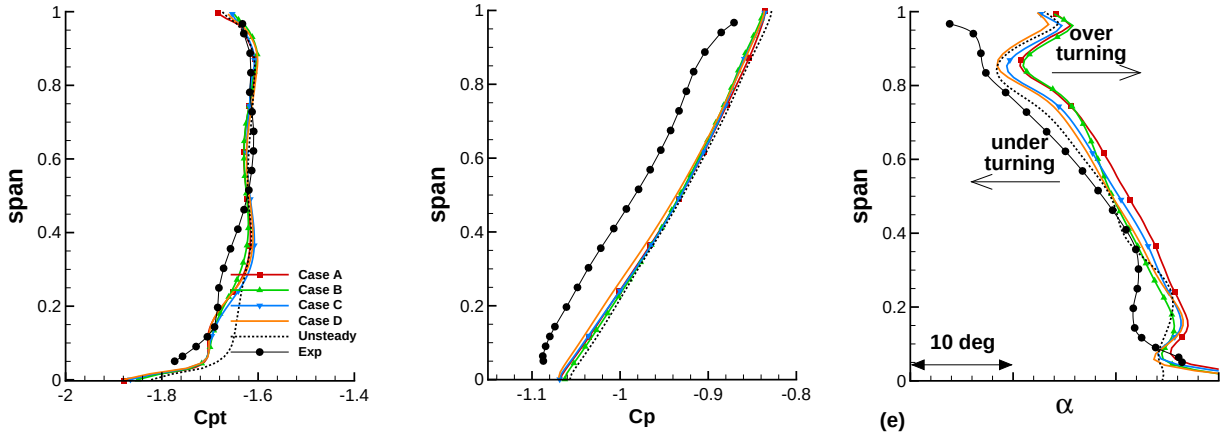

(a) Total pressure (b) Static pressure (c) Yaw angle

Figure 5: Plane F - Spanwise mass-averaged distributions downstream of the LP rotor

TMTF exit flow

In Figure 4 the mass-weighted spanwise distribution of total pressure (a), static pressure (b) and yaw angle (c) at the TMTF outlet (Plane E in Figure 1) are plotted.
The flow leaving the TMTF is subjected to a radial hub-to-shroud pressure gradient that pushes the field towards the hub (Figure 4). This gradient is generated by the swirl effect imposed by the turning strut and by the second bend of the S-shaped diffuser (Spataro et al (2012)).
Unsteady measurements (Lengani et al (2012a)) as well as a steady simulation of the second stage (Spataro et al (2012)), showed that the structures of the HP rotor are convected through the channel and can be visualized at the TMTF exit plane.

All the cases provide a good prediction in this plane in terms of total pressure (Table 3 shows an error below 1%). The static pressure in Figure 4(b) is slightly overestimated for Case B and C, while Case D shows the maximum displacement with the experimental data. The unsteady CFD provides the best overall agreement with the measurements in this plane.

The yaw angle distribution in Figure 4(c) shows no remarkable differences between the different CFD cases. Generally, the CFD appears underestimating the flow turning imposed by the struts. On the other hand, the simulations show more pronounced effects of secondary structures on the flow under and over turnings. Such differences in the yaw angle where already highlighted by Wallin et al

(2011) who presented pre- and post-test prediction results about the flow in this machine together with another TMTF setup.

LP Rotor exit flow

Moving downstream of the LP rotor, measurements were conducted in Plane F (Figure 1). Figure 5 shows the mass-weighted spanwise distribution of total pressure 5(a), static pressure 5(b) and yaw angle 5(c) in Plane F.

Figure 5(b) reveals the effect of the second bend of the S-shaped channel as well as of the LP rotor swirl on the hub-to-shroud pressure gradient responsible for pushing the low energy structures towards the hub.

Moreover, the flow in this region is characterized by a high level of unsteadiness. The perturbations due to the HP rotor in terms of velocity and flow angle are negligible in this downstream plane. Indeed, the largest fluctuations of velocity are due to the TMTF-LP rotor interaction, they occur in the wake and secondary flows of the TMTF. Large fluctuations of static and total pressure are instead due to both rotors to the same extent. Details on the flow field in this region can be found in Lengani et al (2012a,b).

Case B, C and the Unsteady solution appear to provide a very good agreement on the distributions.

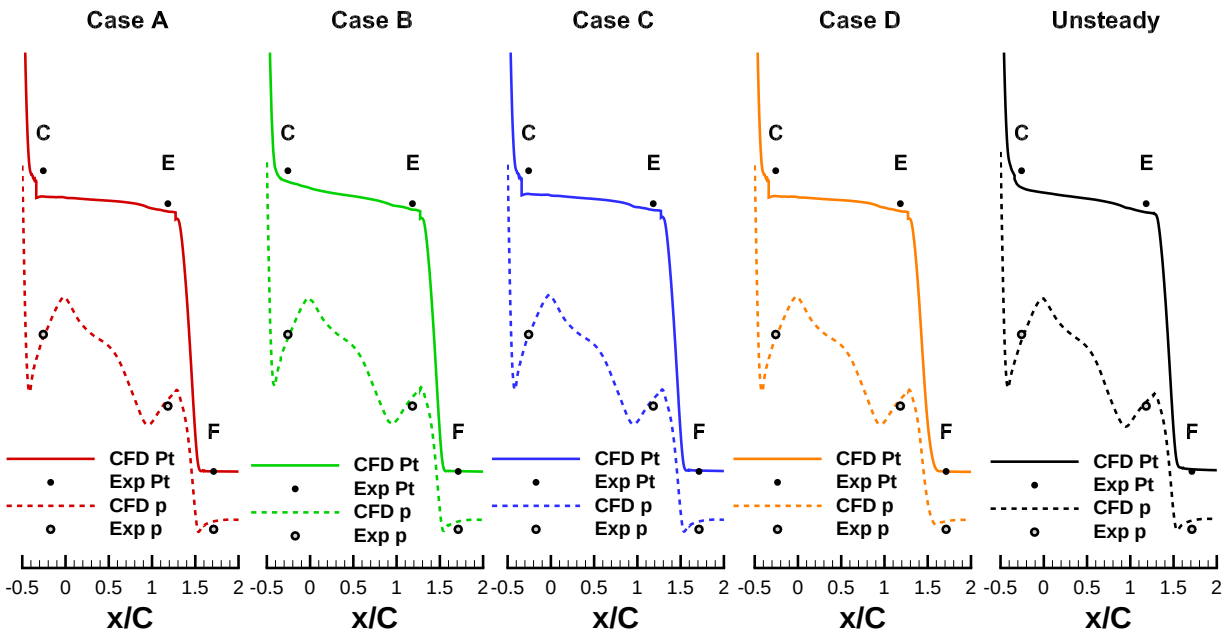

Figure 6: Streamwise total and static pressure evolution along the duct

Flow quantities distribution along the streamwise direction

In order to make a summary of this analysis and to have an idea of the streamwise loss development, Figure 6 reports the comparison between measured and the circumferentially averaged calculated data of total pressure and static pressure along the duct. It is important to notice here that the experimental data are obtained averaging over 95% of the full span, that means that the wall boundary layers are excluded from the averaging process, resulting in a slighty overestimated total pressure.

The axial coordinate x is normalized using the TMTF midspan axial chord C. Generally, the total pressure curves show two vertical drops for $x/C < -0.4$ and $x/C > 1.6$, induced by the work extracted by the rotors, while the horizontal segment $-0.4 < x/C < 1.6$ indicates the inter-turbine

diffuser. In an ideal case (inviscid flow) the total pressure would not change through the TMTF. In reality, viscous effects (i.e. wake mixing or structures propagation) take place and they will induce a slope in this curve. Therefore, the stronger is the slope, the stronger is the local loss.

Comparing the numerical predictions with the experimental data, Figure 6 shows how the trend in evolution of the total pressure is well captured by Case B and the Unsteady CFD. This is due to the use of frozen rotor (Case B) or sliding plane (Unsteady case) located at $x/C = -0.4$ (Interface II Figure 1), where the idea was to model the evolution of the HP rotor structures (tip leakage vortex, lower passage vortex,...) entering the duct. All other cases (A,C and D) show a jump at interface II (Figure 1) caused by the mixing plane. Therefore, performance prediction appears to be overestimated in those cases where the assumption of mixed out flow at the duct inlet is assumed.

The dashed lines in Figure 6 show the propagation of averaged static pressure. Looking at the axial coordinates it is possible to see how the flow recovers pressure within the clean diffusing duct, while the drop which appears between $0 < x/C < 1$ is due to the acceleration induced by the turning TMTF struts.

Table 3: Numerical performance prediction comparison

	Total pressure ($\Delta p_T\%$)			**Static pressure** ($\Delta p\%$)			**TMTF efficiency ($\Delta\eta\%$)**
	Plane C	Plane E	Plane F	Plane C	Plane E	Plane F	Plane C - Plane E
Case A	-2.05%	0.61%	0.01%	0.01%	0.50%	0.82%	8.01%
Case B	-0.93%	-0.45%	0.03%	-0.09%	0.73%	0.81%	1.91%
Case C	-1.85%	-0.49%	0.10%	0.23%	0.54%	0.81%	7.51%
Case D	-2.02%	-0.58%	-0.02%	0.05%	0.52%	0.78%	8.00%
Unsteady	-1.33%	-0.71%	0.23%	-0.54%	0.39%	0.96%	2.79%

In order to complete the comparison with a quantitative estimation of the errors, Table 3 reports the percentage difference of total pressure and static pressure for each measurement plane defined as:

$$\Delta p_T\% = \frac{\bar{p}_{T,cfd} - \bar{p}_{T,exp}}{\bar{p}_{T,exp}} \cdot 100 \tag{3}$$

$$\Delta p\% = \frac{\bar{p}_{cfd} - \bar{p}_{exp}}{\bar{p}_{exp}} \cdot 100 \tag{4}$$

Moreover, in the same table, assuming incompressible flow in the duct (since $Ma_{TMTF} < 0.6$), the error in estimating the efficiency is reported. This is defined as follows:

$$\eta = \frac{\bar{p}_{T,C} - \bar{p}_{T,E}}{\bar{p}_{T,C} - \bar{p}_E} \rightarrow \Delta\eta\% = \frac{\eta_{cfd} - \eta_{exp}}{\eta_{exp}} \cdot 100 \tag{5}$$

Table 3 shows how the use of mixing planes in steady simulation (Case A, C and D) leads to the bigger errors in terms of absolute total and pressure level prediction (difference between experiments and numerical prediction of the duct efficiency between 7.5% and 8.01%). The setups where the rotor structures is not assumed to be mixed out at the duct inlet show a consistent improvement for the performance evalutation: the difference in estimating the pressure level is generally below 1% and for the duct efficiency the error is limited to 1.91% and 2.79% for Case B and Unsteady CFD respectively.

CONCLUSIONS

Several numerical simulations of a two-stage two-spool transonic turbine with turning struts between the rotors were undertaken. A special focus was put on the loss development through the LP

stage. The results were compared with measurements performed in three different planes (downstream of the HP stage, at the LP rotor inflow and at the LP rotor outflow respectively) in terms of spanwise total pressure, static pressure and yaw angle distribution as well as with the strut blade loading at midspan.

A baseline case where all the interfaces were set as mixing plane (Case A) was compared with other three steady simulations set with different domain interface options (Case B, C, D). Moreover the time-averaged flow of an unsteady simulation was analysed.

The comparison of the first measuring plane (Plane C - downstream of the transonic stage) shows problems for the CFD in predicting the quantities distribution at the lower half of the channel (where the stator-rotor interaction is more critical) and at the tip leakage region. The best agreement in terms of quantities distributions in this plane is anyway reached by the unsteady computation.

The comparison at the TMTF exit flow (Plane E) shows no remarkable differences between the CFD cases in terms of yaw angle, but a still appreciable offset can be seen in the pressure distributions.

The strut blade loading at midspan is found best predicted by Case B and Unsteady CFD.

The results from this numerical comparison show that before starting a simulation aimed to predict the aerodynamic performance of a similar setup, a careful choice of the CFD settings should be conducted. In particular, a calculation set in order to minimize the computational cost (i.e. computing one passage per domain and placing mixing planes) could induce large errors in modeling the real flow field.

A comparison about the streamwise evolution of mass averaged total pressure and static pressure show that the use of interfaces which do not mix out the flow field downstream of the rotors (i.e. frozen rotor, or sliding plane) has a remarkable positive effect on the performance prediction.

A promising research for a correct prediction of unsteady effects as well as a reduction of computational costs consists in the development of numerical methods which apply chorochronic (time-space) periodicity in order to reduce the domain extensions (i.e. phase-lagged and time-inclined approaches).

ACKNOWLEDGEMENTS

The authors would like to thank H. Peter Pirker, Josef Hubinka and Berardo Paradiso (currently affiliated at Politecnico di Milano) for the important support during the experimental campaign. This work was financed by the European Union within the EU-project DREAM (contract No. ACP7-GA-2008-211861) in which the LP stage was designed, manufactured and operated.

References

Adamczyk J (1985) Model equation for simulating flows in multi stage turbomachinery. In: Proceedings of the ASME Turbo Expo 1985, ASME Paper No. 85-GT-226

ANSYS (ed) (2010) ANSYS CFX-Solver Modeling Guide. ANSYS

Arnone A, Pacciani R (1996) Rotor-stator interaction analysis using the navier-stokes equation and a multigrid method. ASME Journal of Turbomachinery 118:679–689

Dénos R, Paniagua G (eds) (2005) Effects of Aerodynamic Unsteadiness in Axial Turbomachines. VKI Lecture Series, LS 2005-03

Dénos R, Arts T, Paniagua G, Michelassi V, Martelli F (2001) Investigation of the unsteady rotor aerodynamics in a transonic turbine stage. ASME Journal of Turbomachinery 123:81–89

Erhard J, Gehrer A (2000) Design and construction of a transonic test turbine facility. In: Proceedings of ASME Turbo Expo 2000, May 8-11, Munich, Germany, GT-48

Gaetani P, Persico G, Dossena V, Osnaghi C (2007) Investigation of the flow field in a high-pressure turbine stage for two stator-rotor axial gaps-part 2: Unsteady flow field. ASME Journal of Turbomachinery 129:580–590

Hubinka J, Santner C, Paradiso B, Malzacher F, Göttlich E (2009) Design and construction of a two shaft test turbine for investigation of mid turbine frame flows. In: Proceedings of ISABE 2009, Montreal, Quebec, Canada, ASME Paper No. ISABE-2009-1293

Hubinka J, Paradiso B, Santner C, Pirker HP, Göttlich E (2011) Design and operation of a two spool high pressure test turbine facility. In: Proceeding of the 9th ETC conference, Instambul, Turkey, pp 1531-1540

Lavagnoli S, Yasa T, Paniagua G, Duni S, Castillon L (2012) Aerodynamic analysis of an innovative low pressure vane placed in a s-shape duct. ASME Journal of Turbomachinery 134(2):011,013 (13 pages)

Lengani D, Santner T, Spataro R, Paradiso B, Göttlich E (2012a) Experimental investigation of the unsteady flow field downstream of a counter-rotating two-spool turbine rig. In: Proceedings of ASME Turbo Expo 2012, June 11-15, Copenhagen, Denmark, ASME Paper No. GT-GT2012-68583

Lengani D, Selic T, Spataro R, Marn A, Göttlich E (2012b) Analysis of the unsteady flow field in the turbines by means of modal decomposition. In: Proceedings of ASME Turbo Expo 2012, June 11-15, Copenhagen, Denmark, ASME Paper No. GT-GT2012-68582

Meneveau C, Katz J (2002) A deterministic stress model for rotor-stator interactions in simulations of average-passage flow. ASME Journal of Fluids Engineering 124:550–554

Menter FR (1994) Two-equation eddy-viscosity turbulence models for engineering applications. AIAA Journal 32(8):1598–1605

Miller RJ, Moss RW, Ainsworth RW, Harvey NW (2003a) The development of turbine exit flow in a swan-necked inter-stage diffuser. In: Proceedings of ASME Turbo Expo 2003, June 16–19, Atlanta, Georgia, USA, ASME Paper No. GT-2003-38174

Miller RJ, Moss RW, Ainsworth RW, Horwood CK (2003b) Time-resolved vane-rotor interaction in a high-pressure turbine stage. ASME Journal of Turbomachinery 125:1–13

Persico G, Mora A, Gaetani P, Savini M (2010) Unsteady aerodynamics of a low aspect ratio turbine stage: modelling issues and flow physics. In: Proceedings of ASME Turbo Expo 2010, June 14-18, Glasgow, UK, ASME Paper No. GT2010-22927

Rhie C, Gleixner A, Spear D, Fischberg C, Zacharias R (1995) Development and application of a multistage navier-stokes solver:part1-multistage modeling using body forces and determinsitic stresses. ASME Journal of Turbomachinery 120:205–229

Santner C, Paradiso B, Malzacher F, Hoeger M, Hubinka J, Göttlich E (2011) Evolution of the flow through a turning mid turbine frame applied between a transonic hp turbine stage and a counter-rotating lp turbine. In: Proceedings of 9^{th} European Turbomachinery Conference, March 21-25, Istanbul, Turkey, Paper No. 110

Spataro R, Santner C, Lengani D, Göttlich E (2012) On the flow evolution through a lp turbine with wide-chord vanes in an s-shaped channel. In: Proceedings of ASME Turbo Expo 2012, June 11-15, Bella Center, Copenhagen, Denmark, ASME Paper No. GT-2012-68178

Tucker P (2011) Computation of unsteady turbomachinery flows:part 1 - progress and challenges. Progress in Aerospace Sciences 47:522–545

Wallin F, Ore S, Göttlich E, Santner C (2011) Aero-design and validation of a turning mid turbine frame. In: Proceedings of ISABE 2011, September 12-16, Gothenburg, Sweden, ISABE Paper No. ISABE-2011-1713

Yasa T, Lavagnoli S, Paniagua G (2011) Impact of a multi-splitter vane configuration on the losses in a 1.5 turbine stage. Proceedings of IMechE Vol 225 225:964–974